Plasmons in core-level photoemission spectra of Al(111)

C. Biswas, A. K. Shukla, S. Banik, V. K. Ahire, and S. R. Barman*
Inter University Consortium for Department of Atomic Energy Facilities, Khandwa Road, Indore, 452017, Madhya Pradesh, India
(Received 3 December 2002; published 28 April 2003)

The line shape and intensity of surface and bulk plasmon excitations in Al $2s$ and $2p$ core-level spectra of Al(111) have been studied as functions of the photoelectron emission angle (θ). For both surface and bulk plasmons, an asymmetric line shape is observed in normal emission, which becomes more symmetric in grazing emission. The asymmetric line shape is in good agreement with theory. The relative contributions of the intrinsic, extrinsic, and interference processes to the surface plasmon intensity are determined from its variation with θ and from theoretical line-shape calculations. We show the importance of the interference process in determining the intensity and line shape of the plasmons. From the intensity variation of multiple ($n=1-6$) bulk plasmons ($n\omega_p$) with n, the intrinsic and extrinsic bulk plasmon probabilities are determined.

DOI: 10.1103/PhysRevB.67.165416 PACS number(s): 82.80.Pv, 73.20.Mf, 79.60.Bm, 79.60.−i

I. INTRODUCTION

The origin of collective plasmon excitations in the photoemission spectra of metals has been a topic of extensive experimental and theoretical investigation from the early days of photoemission.[1–24] Bulk plasmons are longitudinal oscillation modes of the electron gas in the solid, and are given by the condition $\epsilon=0$, where ϵ is the bulk dielectric function. The surface plasmon is an oscillating sheet of charge located at the surface, although its energy is dictated by the bulk property ($\epsilon=-1$). In the direction perpendicular to the surface, the charge distribution of the surface plasmon has a monopolar character, and hence it is referred to as the monopole surface plasmon.[25,26] The physics of plasmon excitations in photoemission is enriched by the different processes that contribute to its intensity. The sudden change in the potential due to the formation of a core hole attracts the conduction electrons to screen the core-hole resulting, in the *intrinsic plasmon* excitation.[1,2] On the other hand, the *extrinsic plasmon* excitation is created by the Coulomb interaction of the conduction electrons with the photoelectron traversing through the solid from the photoemission site to the surface. Besides, an *interference* process occurs due to the quantum interference between the intrinsic and extrinsic plasmons. The interference effect can be visualized as the interaction between the localized photohole (intrinsic) and the outgoing photoelectron (extrinsic) in which the virtual plasmons created by one is absorbed by the other.[2]

In order to study the importance of these effects, Pardee *et al.*[3] carried out x-ray photoemission spectroscopy studies on Al, Na, and Mg $2s$ peaks, and came to the conclusion that the intrinsic effect was almost absent using a random spatial emission model for the excitation of plasmons.[15] This was in contradiction with theoretical results which predicted the existence of the intrinsic plasmon.[1,2,20] Fuggle *et al.* tried to resolve the issue by studying Al layers deposited on Mn, and found some evidence for the intrinsic plasmon, although quantitative estimates could not be extracted.[4] van Attekum *et al.* studied the variation of successive bulk plasmon ($n\omega_p$) intensity in Al $2s$, and concluded that about 25% of the bulk plasmon intensity is due to the intrinsic plasmon.[5] Based on a similar study of Al $2p$ and $2s$ core levels, Steiner *et al.* found the intrinsic plasmon contribution to be about 14%.

The dependence of plasmon intensities in polycrystalline Al as a function of the photoelectron emission angle (θ) has been studied by Baird *et al.*[8] The authors found that the surface plasmon intensity is markedly enhanced at low θ, but they did not report any change in the plasmon line shape as a function of θ.[8] They determined the intensity variations of $1\omega_p$, $2\omega_p$, and $1\omega_s$, and compared them with theoretical calculations based on a jellium model. The authors found that, although the trend is similar, the theoretical values are higher than the corresponding experimental values.[8] Bradshaw *et al.* studied the oxygen $1s$ core-level spectra of 0.17-ML oxygen chemisorbed on Al(111). The loss structure of O $1s$ showed only an Al related surface plasmon, and a bulk plasmon was not observed. On the basis of semiclassical calculations, the authors suggested that in the high photoelectron velocity limit, the intrinsic and interference contributions are independent of θ and that the extrinsic contribution varies as $1/\sin\theta$. They found a small intrinsic plasmon contribution to the surface plasmon intensity.

Many theoretical studies have been performed to evaluate the contribution of the intrinsic and extrinsic processes and to understand their origin in photoemission.[1–2,14–23] Chang and Langreth treated the inelastic plasmon losses as a many body effect in the photoemission process, and included the effects of the solid surface and the core hole.[2,14] Šunjić *et al.* used an electron-plasmon interaction model for fast electrons and considered the effect of localized core holes to provide a quantitative description of multiple bulk and surface plasmon processes in metals.[18,19] Feibelman calculated the plasmon intensities as a function of depth and θ, assuming an infinite core-hole lifetime and a smooth cutoff at the critical wave vector.[16] Penn discussed a three step theoretical model for plasmon losses in photoemission including the effects due to electron-electron scattering and plasmon dispersion, but the interference effect was not included.[20] Penn calculated the plasmon line shapes and estimated the intrinsic bulk plasmon contribution to be 26% for Al,[20] which was much lower than 50% intrinsic plasmon contribution suggested by Lundqvist.[1] While the earlier studies[7,15,18,19] assumed a classical trajectory for the outgoing electron and neglected plasmon dispersion, Inglesfield used the golden rule formalism of photo-

emission and considered plasmon dispersion as well as the interference effect. Inglesfield studied the suppression of the plasmon intensities at low electron kinetic energies by calculating the plasmon line shapes as functions of the kinetic energy and depth (z) of the photoemission site.[21,22] The interference between the extrinsic and intrinsic plasmons was found to suppress the long wavelength plasmon excitations.[21,22] Using a transition-matrix approach, Bose *et al.*[23] calculated the line shape and intensity of the intrinsic, extrinsic, and interference contributions to both bulk and surface plasmons as functions of z, and their results are in good agreement with that of Inglesfield.[22] The theory by Bose *et al.* can be extended to the $z<0$ situation for the problem of photoemission from adsorbed atoms on surfaces. The theoretical calculations by different groups[20,22,23,24] predict asymmetric line shapes for both bulk and surface plasmon.

Although plasmon excitations in photoemission have been known for more than three decades, and were studied by different groups in the late 1970s and early 1980s, there still remain unresolved issues which need to be investigated. For example, a wide disagreement exists in the literature about the strength of the intrinsic bulk plasmon (from 10% to 50%) in Al, which is an ideal test system for different theories because of its nearly free electron nature. On the basis of plasmon line-shape calculations,[23] the importance of the interference effect has been suggested, but it still remains to be studied experimentally. van Attekum *et al.* reported an asymmetric plasmon line shape from photoemission; but in contrast the line shape measured by electron energy loss spectroscopy (EELS) was found to be symmetric.[5,27] The reason for the difference in plasmon line shapes between photoemission and EELS is still unexplained. The line shape of the plasmons, which is expected to be asymmetric, and change with the photoelectron velocity (v) and depth z from which the photoemission takes place, has not been studied experimentally to date. Since the relative contributions of the different processes are expected to change as functions of the emission angle, we have studied the θ dependence of the plasmon excitations in the Al $2s$ and Al $2p$ core levels of Al(111) using x-ray photoemission spectroscopy (XPS). The experimentally obtained surface plasmon line shape has been compared with theoretical results calculated following the perturbation based method of Inglesfield.[21,22] From the variation of the surface plasmon intensity with θ, we have determined the different contributions to the surface plasmon on the basis of the theoretical model by Bradshaw *et al.*[7] Because of the disagreement in the literature about the strength of the intrinsic bulk plasmon, the intensity variation of multiple bulk plasmons ($n\omega_p$) have been studied as functions of n and the intrinsic and extrinsic plasmon contributions have been determined based on theoretical work by Chang and co-workers.[14,17]

II. EXPERIMENT AND DATA ANALYSIS

The experiments were performed at a base pressure of 6×10^{-11} mbar using a commercial electron energy analyzer (Phoibos100 from Specs GmbH, Germany) and a nonmonochromatic Mg$K\alpha$ laboratory x-ray source. An electropolished Al(111) crystal was cleaned by repeated cycles of sputtering using 1–2 KeV Ar^+ ions and subsequent annealing at 450 °C to regenerate surface order. The surface order was monitored through low energy electron diffraction (LEED), and a 1×1 LEED pattern was observed for the clean surface. The analyzer angular resolution was 3°, the pass energy was set at 5 eV, and a slit size of 6 mm diameter was used. Thus the energy resolution of the analyzer (ΔE_{ana}) is about 0.15 eV. The emission angle was varied by rotating the sample. $\theta=90°$ and 0° spectra could not be recorded due to geometrical restrictions in the experimental chamber. Hence, in an approximate sense, we refer to $\theta=80°$ to be normal emission and $\theta=10°$ to be grazing emission. It should be noted that the change in electron propagation angle from inside the crystal to vacuum due to refraction effect at the surface is not significant at large photon energies and the studied θ range of the present experiment.[8]

Since the spectra have been recorded with nonmonochromatic Mg$K\alpha_{1,2}$ radiation, the features due to the Mg$K\alpha_{3,4}$ satellite lines have been subtracted using a routine assuming that the satellites produce a replica spectrum as the main line, but shifted and reduced in intensity.[28] The inelastic background was subtracted using the Tougaard method.[29] The Al $2s$ and $2p$ core-level spectra were fitted with the Doniach-Šunjić (DS) line shape[30] using a least square error minimization routine based on the Levenberg-Marquardt algorithm. Initially, only the Al $2p$ main peak region (69.6–78.6 eV binding energy; Fig. 2) was fitted in order to determine the main peak related parameters. The Al $2p$ main peak includes both the spin-orbit components, which are not clearly resolved due to inadequate resolution in the present work. The experimentally reported value of the spin-orbit splitting for Al $2p$ is 0.411 eV, which has been determined from well resolved Al $2p_{3/2}$ and Al $2p_{1/2}$ peaks.[31] The experimentally determined intrinsic lifetime width [full width at half maximum (FWHM)] of the DS line shape is reported to be 0.03 eV.[31] In our fitting scheme, we fix the spin-orbit splitting and DS lifetime broadening to be 0.41 and 0.03 eV, respectively. The DS asymmetry parameter and the lifetime broadening have been taken to be same for both spin-orbit components. Ideally, the statistical branching ratio between $2p_{3/2}$ and $2p_{1/2}$ should be 2, but this is allowed to vary since the branching ratio could be different for various reasons like different bondings of the surface atoms, different radial wave functions leading to different dipole matrix elements, and difference in the photoionization cross section due to a slight difference in the kinetic energies of the electrons from the different spin-orbit split levels.[32] From the fitting, we obtain the branching ratio to be 1.7. The DS asymmetry parameter was obtained to be 0.11 ± 0.01 for Al, which is in agreement with the existing literature.[31,33]

In order to account for the instrumental factors (i.e. the analyzer and the photon source related broadenings), the Doniach-Šunjić line shape has been convoluted with a Voigt function. The FWHM of the Voigt function (ΔE) for each spin-orbit component is found to be 0.6 eV. Since $\Delta E=\sqrt{(\Delta E_{\text{ana}}^2+\Delta E_{\text{photon}}^2)}$, ΔE_{photon}, which is the broadening due to the Mg$K\alpha_{1,2}$ source, turns out to be 0.58 eV (ΔE_{ana}

$=0.15$ eV). It should be noted that this value is in fair agreement with the previously reported linewidth of 0.7 eV for Mg$K\alpha_{1,2}$.[34] The instrument related broadening has been kept fixed while fitting the Al $2s$ spectra, which was recorded with the same analyzer setting as Al $2p$.

The whole range (as shown in Fig. 2), including the main peak and the plasmon region, has been fitted, and extra weightage was given to the plasmon region. The plasmon peaks have been fitted with asymmetric Lorentzian functions convoluted with the instrumental broadening. The form of the asymmetric Lorentzian function is given by

$$\frac{I_o}{1+[(E_K-E_K^p)/\Gamma(E)]^2}, \tag{1}$$

where the half width at half maximum (HWHM), $\Gamma(E)$, is equal to Γ_R when $E_K>E_K^p$ (E_K^p is the peak position in the kinetic energy scale, E_K) and $\Gamma(E)=\Gamma_L$ when $E_K<E_K^p$. Thus Γ_R and Γ_L are the right and left Lorentzian widths, respectively, and I_o is the intensity. The choice of asymmetric Lorentzian for simulating the plasmon line shape is based on results of previous theoretical calculations,[20,22,23,24] and has been used in the literature before.[5] The asymmetric Lorentzian widths (Γ_R and Γ_L) are allowed to vary independently in the fitting routine. In the case of Al $2p$, the plasmon peak is regarded as the sum of the contributions from Al $2p_{3/2}$ and $2p_{1/2}$ spin-orbit components, and two separate asymmetric Lorentzians are considered for each plasmon peak separated by the spin-orbit splitting. The widths of these two components are constrained to be equal. The asymmetric plasmon line shape has been convoluted with the same Voigt function obtained from the fitting of the Al $2p$ core-level spectrum, and the instrumental broadening parameters have not been varied. Thus the deconvoluted plasmon line shapes are obtained by separating out the effect of instrumental broadening through the fitting procedure.

III. RESULTS AND DISCUSSION

A. Experimental plasmon line shapes

Al $2s$ spectra, recorded at nearly normal (80°) and grazing (10°) emissions, are shown in Fig. 1. The striking difference is a large enhancement by a factor of about 5 in the intensity of the monopole surface plasmon ($1\omega_s$) in the grazing emission at 128.4 eV binding energy (BE) or a 10.4 eV loss energy. From the deconvoluted $1\omega_s$ line shape, it is evident that besides the intensity enhancement, there is a drastic change in the line shape between normal and grazing emissions (shifted thick solid lines in Fig. 1). In normal emission, the surface plasmon has an unusual shape with a gradually decreasing intensity towards the higher loss energy (or BE) side and a steplike line shape on the lower loss energy side (marked by arrow in Fig. 1). The corresponding left and right Lorentzian widths, Γ_L and Γ_R, obtained from the least-square fitting, are 3.6 and 0.08 eV, respectively. In contrast, in grazing emission the surface plasmon is relatively more symmetric, although Γ_L ($=1.92$ eV) is still larger than Γ_R ($=0.84$ eV). In contrast to the surface plasmon, the bulk plasmon ($1\omega_p$) intensity decreases in the grazing emission by a factor of 2.4 compared to normal emission. In fact, the intensity of the surface plasmon is more than that of the bulk plasmon in the grazing emission, which was not observed in previous studies.[7,8] This is probably related to the clean Al(111) surface in the present work, where the oxygen $1s$ signal is in the noise level, compared to the residual oxygen contamination reported in previous studies.[7,8] Thus even a small amount of contamination on the surface can affect the surface plasmon intensity, especially in the grazing emission geometry.

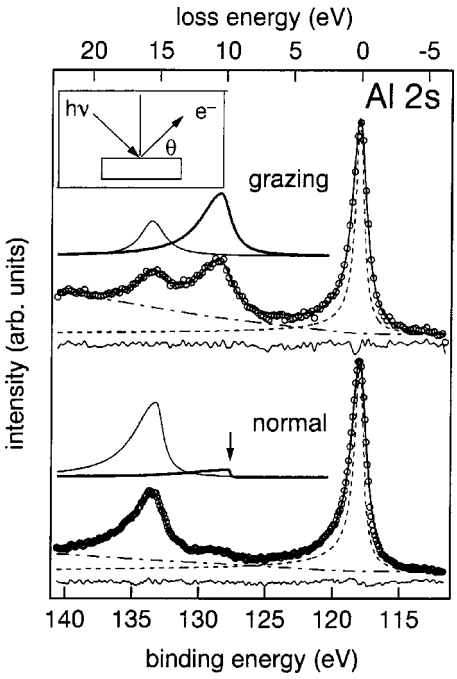

FIG. 1. Comparison of the surface ($1\omega_s$) and bulk ($1\omega_p$) plasmon features in the photoemission spectra of Al $2s$ recorded in nearly grazing (10°) and normal (80°) emissions. The no-loss main peaks in both the spectra are normalized to the same height. The solid line through the experimental data (open circles) is the fitted curve. The residual for the fit, which is within the statistical scatter of the experimental data, is shown below each spectra. The deconvoluted Al $2s$ Doniach-Šunjić line shape (dashed line) and the inelastic background (dot-dashed line) are also shown. The surface (thick solid line) and bulk (thin solid line) plasmon line shapes are shifted upwards for clarity of presentation. The steplike surface plasmon line shape is indicated by an arrow. The inset shows the geometry of the experiment.

The systematic change in the plasmon line shape and intensity for different θ is shown in Fig. 2 for both Al $2s$ and $2p$ core-level spectra of Al(111). The Al $2s$ ($2p_{3/2}$) no-loss main peak occurs at 118 (72.8) eV BE. The main peaks do not exhibit any change in the line shape with θ. In normal emission, for both Al $2s$ and $2p$, $1\omega_s$ exhibits a steplike line shape at 9.6 eV loss energy (indicated by arrows in Fig. 2) while towards the higher loss energy side a gradual decrease in intensity is observed. As θ decreases, the steplike shape becomes smoother, as shown by the systematic variation of Γ_R and Γ_L in Fig. 3. For Al $2s$, Γ_R remains small between 80° to 40°, and for smaller emission angles increases rapidly to 0.84 eV [Fig. 3(a)]. In Al $2p$, Γ_R increases almost linearly

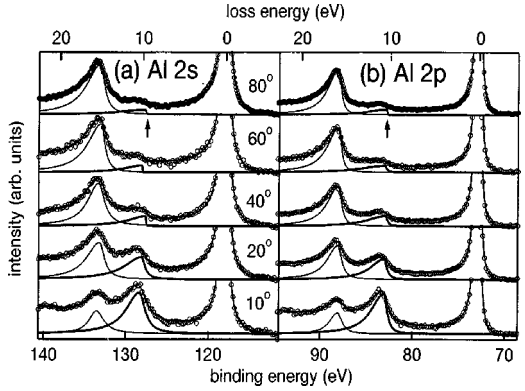

FIG. 2. (a) Al $2s$ and (b) Al $2p$ core-level spectra as functions of the emission angle (θ). The solid line through the experimental data (open circles) is the fitted curve. The no-loss main peaks (normalized to same height) are truncated to show the plasmon peaks ($1\omega_s$: thick solid line; $1\omega_p$: thin solid line) in an expanded scale. Arrows show the positions of the steplike surface plasmon line shape.

to a maximum value of about 0.4 eV. Thus the trend of increasing Γ_R from normal to grazing geometry is evident for both Al $2s$ and $2p$. In contrast, Γ_L exhibits a decreasing trend with θ and are larger than Γ_R values [Fig. 3(b)]. For Al $2s$, Γ_L decreases from about 3.5 eV for $\theta=80°$ to about 2 eV for $\theta=10°$. Γ_L for Al $2p$ also shows a similar trend. At higher θ, the fact that the surface plasmon is less intense (and hence the statistical scatter in the spectra becomes more important), compounded with the uncertainty in the Γ_R parameter of the bulk plasmon (with which it overlaps), enhances the uncertainty in the surface plasmon Γ_L (Fig. 3, lower panels) However, despite the scatter in a few data points, the trend in the Γ_L values is quite clear for both Al $2s$ and Al $2p$. We quantify the observed asymmetric line shape by an asymmetry parameter, $\kappa=\Gamma_L/\Gamma_R$. Thus $\kappa=1$ would imply

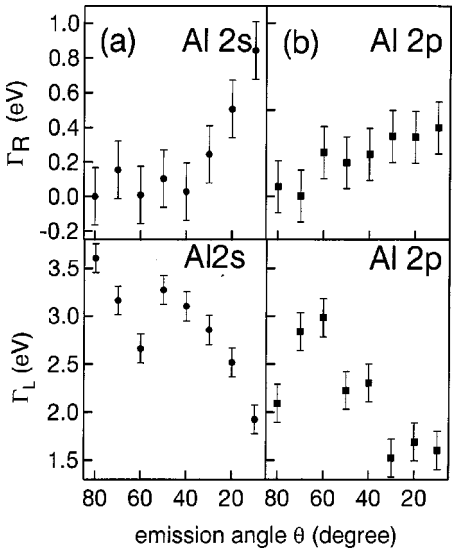

FIG. 3. Surface plasmon right (Γ_R) and left (Γ_L) Lorentzian widths for (a) Al $2s$ (filled circles) and (b) Al $2p$ (filled squares) as functions of θ.

a symmetric Lorentzian line shape, while increasing the deviation from unity would imply a larger asymmetry. From normal to grazing emission, κ decreases for both the core levels, for example in Al $2s$ it decreases from 45 to about 2. Thus in Al(111), the surface plasmon gradually changes from highly asymmetric to more symmetric line shape with decreasing θ, as observed for both Al $2s$ and $2p$ core-level spectra.

Although not as pronounced as the surface plasmon, the bulk plasmon line shape is also somewhat asymmetric in normal emission, e.g., for Al $2s$ ($2p$) $\Gamma_L=2.0$ (1.3) eV, while $\Gamma_R=0.63$ (0.32) eV with $\kappa=3.2$ (4.1). As θ decreases, $1\omega_p$ becomes more symmetric, and in grazing emission we obtain, for Al $2s$ ($2p$), $\Gamma_L=1.09$ (0.98) eV, while $\Gamma_R=1.11$ (0.6) eV when $\kappa=0.98$ (1.7). Thus the bulk plasmon also shows a similar trend as the surface plasmon of becoming more symmetric with decreasing θ and becomes nearly symmetric in grazing emission.

B. Surface plasmon line-shape calculation

In order to compare the experimental data with theory and to evaluate the extrinsic, intrinsic, and interference contributions, we have calculated the $1\omega_s$ line shape following the perturbation based method suggested by Inglesfield.[21,22] Inglesfield performed the calculations for normal emission geometry using the golden rule formulation. The surface and bulk plasmon line shapes were calculated as functions of the incident photon energy and depth z from which the photoemission is occurring. The final state is comprised of the outgoing photoelectron, the localized core hole, and the possible plasmon excitations. The interaction of photoelectrons with plasmons was treated by first order perturbation theory. Since Al is a nearly free electron metal, a free electron model was used for the solid, and the dispersion of the plasmon frequency with momentum was considered in the calculation. Using the following expression given by Inglesfield for $1\omega_s$ photocurrent,[22] we have calculated the Al $2s$ surface plasmon line shape $[J_{\rm tot}(\epsilon_x,\omega,z)]$ corresponding to photoemission from a depth z for the 1253.6 eV incident photon energy used in the present work:

$$J_{\rm tot}(\epsilon_x,\omega,z)=\frac{\omega_s}{\delta}|w_1-w_2-w_3|^2, \tag{2}$$

where

$$w_1=x_1+iy_1=\frac{2ik_\parallel\exp\{-i[2\epsilon-k_\parallel^2]^{0.5}z\}}{[2\epsilon-k_\parallel^2]^{0.5}[\{[2\epsilon-k_\parallel^2]^{0.5}-k\}^2+k_\parallel^2]}, \tag{3}$$

$$w_2=x_2+iy_2=\frac{2\exp[-(k_\parallel+ik)z]}{k^2-2\epsilon-2ikk_\parallel}, \tag{4}$$

$$w_3=x_3+iy_3=\frac{\exp[-(k_\parallel+ik)z]}{\omega_{s,k_\parallel}}. \tag{5}$$

In the above equations, k is the photoelectron momentum and $k_\parallel$ is the surface plasmon momentum parallel to the surface. ϵ is the total energy available for the excitation, i.e.,

photon energy (ω) minus the binding energy of the core level. ϵ_x is the loss energy scale defined by $\epsilon-\epsilon_k$, where ϵ_k is the photoelectron energy given by $\frac{1}{2}k^2$ in atomic units. ω_s is the frequency of the surface plasmon for $k_\parallel=0$. $\omega_{s,k_\parallel}$ is the surface plasmon frequency given by the linear dispersion relation $\omega_{s,k_\parallel}=\omega_s+\delta k_\parallel/2$.[35] The total energy available for excitation (ϵ) minus the photoelectron kinetic energy (ϵ_k) is equal to $\omega_{s,k_\parallel}$. Thus $k_\parallel$ can be expressed in terms of loss energy as $(2/\delta)(\epsilon_x-\omega_s)$. Thus $J_{\rm tot}(\epsilon_x,\omega,z)$ is obtained by computing Eq. (2) for different ϵ_x values which corresponds to particular $k_\parallel$ values as given by the above expression. δ is a constant given by $\sqrt{3/5}v_F$, where v_F is the Fermi velocity and is taken to be 0.72 au for Al.[22] The above expression for δ gives the correct bulk plasmon dispersion relation and consistency between hydrodynamic and quantum mechanical calculations.[36]

In Eq. (2), w_1 and w_2 represent the extrinsic terms, while w_3 is the intrinsic term. The final line shape ($J_{\rm tot}$) is obtained by integrating $\exp(-z/\lambda)\times J_{\rm tot}(\omega,z)$ over z, where λ is the inelastic mean free path. $\exp(-z/\lambda)$ is the weighting factor used for integration over z, which implies that a photoelectron, after exciting a plasmon, can excite another plasmon or be scattered through other processes.[22] At an Al $2s$ photoelectron kinetic energy of about 1135.6 eV (corresponding to a 1253.6 eV photon energy), λ is taken to be 24 Å.[37] The convergence of the numerical integration has been tested and the results are in agreement with the lower photon energy calculations performed by Inglesfield.[22]

The experimental Al $2s$ surface plasmon spectrum in normal emission (open circle) is compared with the calculated line shape ($J_{\rm tot}$, thick solid line) integrated over depth z [Fig. 4(a)]. For the purpose of comparing the shapes, the experimental spectrum is normalized to the same height as the theoretical curve which is shifted to align with the experimental spectrum. To take into account the finite lifetime of the plasmon, the theoretical curve has been broadened by $k_\parallel$ dependent Lorentzian function whose HWHM is $\gamma=\gamma_o+gk_\parallel$, where $g=1.3$ eV and $k_\parallel$ is in Å^{-1}.[38] γ_o is taken to be almost zero, which is expected for a free electron metal like Al.[38,39] It should be noted that a large value ($\approx$2 eV) of γ_o has been obtained from EELS experiments on Al(111).[27] Such a large discrepancy of γ_o between theory and EELS has been explained in other systems like Li and Mg to be partly due to the bulk lattice potential.[38] However, in Al such an effect would be negligible, and a free electron jellium model has been successful in explaining the collective excitations in Al.[25] Hence the large γ_o for surface plasmons observed in EELS (where unlike photoemission the electrons are incident on and reflected from the surface) is probably related to the enhanced scattering (since the electron crosses the surface twice) from the defects, steps, phonons, etc. Moreover, in contrast to photoemission, intrinsic plasmons are not produced in EELS and the interference effect is absent.

In agreement with experiment, the calculated surface plasmon line shape $J_{\rm tot}$ is highly asymmetric, and the steplike line shape is well reproduced by the theory [Fig. 4(a)]. However, it should be noted that on the higher loss energy side,

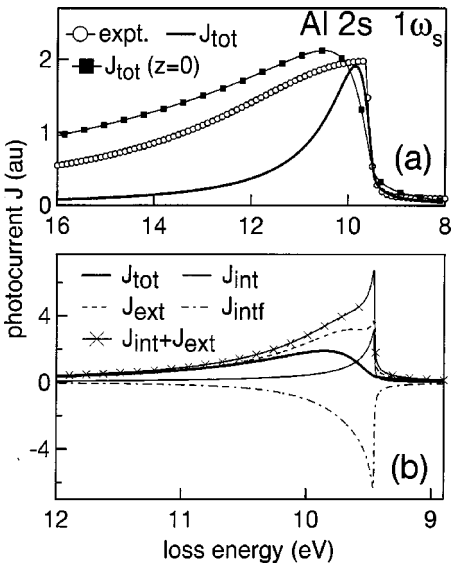

FIG. 4. (a) The calculated surface plasmon line shapes $J_{\rm tot}$ (thick solid line) and $J_{\rm tot}(z=0)$ (filled squares) are compared with the experimental Al $2s$ surface plasmon (open circles) recorded in normal emission. The zero of the loss energy scale (not shown in the figure) refers to the no-loss peak position (b) The calculated total ($J_{\rm tot}$ thick solid line), intrinsic ($J_{\rm int}$, thin solid line), extrinsic ($J_{\rm ext}$, dashed line), interference ($J_{\rm intf}$, dot-dashed line), and sum of extrinsic and intrinsic ($J_{\rm int}+J_{\rm ext}$, crosses) contributions to the Al $2s$ surface plasmon line shape shown in an expanded horizontal scale.

the experimental spectrum has a larger intensity compared to theory [Fig. 4(a)]. To find possible reasons for this disagreement, we have calculated the $1\omega_s$ line shape due to photoemission just at the surface ($z=0$). The calculated $1\omega_s$ line shape [$J_{\rm tot}(z=0)$] has a larger intensity on the higher loss side than the integrated line shape ($J_{\rm tot}$). Thus a possible reason for the disagreement could be that the contribution of surface photoemission (occurring at $z=0$) to the surface plasmon intensity is underestimated by the theoretical curve, $J_{\rm tot}$. This is probably related to the choice of the weighting factor $\exp(-z/\lambda)$, which is based on a semiclassical approach assuming that the bulk extrinsic terms dominate.[22]

Another possible reason for the underestimation of intensity by theory on the higher loss energy side could be related to the existence of the *multipole* surface plasmon, which is a higher order surface mode expected to occur around 13 eV loss energy.[25] The multipole plasmon has been identified in Al by photoyield experiments, where a huge enhancement occurs in the photoemission cross section when the incident photon frequency is equal to the multipole plasmon frequency.[40,41] In contrast to the monopole surface plasmon, the charge distribution of the multipole surface plasmon perpendicular to the surface can have a node, i.e., of dipolar or multipolar form. Parallel to the surface, the behavior of the monopole and mutipole modes are similar. Recently, the multipole surface plasmon mode has been observed in EELS experiments on Al(111) at small $k_\parallel$, and its intensity is found to be about 57% of the monopole surface plasmon.[27] A similar relative intensity of the multipole plasmon may be expected in photoemission. However, no theoretical calcula-

tions exist in the literature for a photoemission-related multipole plasmon line shape. The reason that a separate feature is not observed for the Al multipole plasmon in the present experiments could be that, unlike EELS, contributions from all $k_{\parallel}$'s are observed in photoemission, which probably results in a broad featureless line shape for the multipole plasmon. Thus, although not decisive, the present results indicate that a part of the surface plasmon intensity observed in photoemission could be related to the multipole plasmon.

The intrinsic (J_{int}), extrinsic (J_{ext}), and interference (J_{intf}) contributions, which add up to give the total integrated surface plasmon line shape (i.e., $J_{\mathrm{tot}}=J_{\mathrm{int}}+J_{\mathrm{ext}}+J_{\mathrm{intf}}$), are shown in Fig. 4(b) in an expanded scale. These contributions are given by

$$J_{\mathrm{int}}=x_3^2+y_3^2, \tag{6}$$

$$J_{\mathrm{ext}}=x_1^2+x_2^2-2x_1x_2+y_1^2+y_2^2-2y_1y_2, \tag{7}$$

$$J_{\mathrm{intf}}=-2x_1x_3+2x_2x_3-2y_1y_3+2y_2y_3, \tag{8}$$

where x_i and y_i ($i=1,2,3$) are defined in Eqs. (3)–(5). The intrinsic surface plasmon (J_{int}) is asymmetric with a sharp peak at a 9.45 eV loss energy with a 0.1 eV FWHM. The surprising observation is that the J_{tot} peak intensity is lesser than both intrinsic and extrinsic peak intensities. In fact, the area under J_{ext} (centered around the 9.6 eV loss energy with a 0.7 eV FWHM) is more than J_{tot}. This is because although both the intrinsic and extrinsic terms are positive, the interference contribution (J_{intf}) is negative over the whole energy range. It has an asymmetric inverted peak at 9.45 eV loss energy with a 0.15 eV FWHM. The negative value of the interference term signifies that the plasmons created by the outgoing photoelectron (extrinsic process) is absorbed by the localized photohole potential (intrinsic process), reducing the total intensity of the surface plasmon. In fact, at the minimum loss energy end of the plasmon feature (9.4 eV) the calculated plasmon intensity becomes zero due to the negative interference term. This is because the minimum loss end corresponds to the $k_{\parallel}\rightarrow 0$ limit where the surface plasmons are excited by an average potential of the core hole and the photoelectron, which is zero for $k_{\parallel}=0$.[42] However, this is not valid for shorter wavelength ($k_{\parallel}>0$) surface plasmons, and a large enhancement in intensity is observed with the J_{tot} peak at a 9.85 eV loss energy. For higher loss energies, $k_{\parallel}$ increases since $k_{\parallel}=2/\beta\times(\text{loss energy}-\omega_s)$.[22] But, the probability of exciting shorter wavelength plasmons decreases because it involves a larger momentum transfer from the photoelectrons, and hence the plasmon intensity decreases towards the higher loss energy side. The importance of the interference term in determining the plasmon line shape is clear from the comparison of J_{tot} and $J_{\mathrm{int}}+J_{\mathrm{ext}}$. J_{intf} reduces the $J_{\mathrm{int}}+J_{\mathrm{ext}}$ intensity by 36%, and makes the line shape more symmetric [Fig. 4(b)].

By calculating the area under the respective theoretical curves, the ratio of the intrinsic, extrinsic, and interference surface plasmon contributions is found to be 1:3.6:−1.9, respectively. Thus the extrinsic plasmon intensity is largest, although in normal emission and at high photoelectron velocities, where the electron has less time to interact with the surface, the intrinsic plasmon is expected to dominate. It should be noted that in the case of the surface photoemission contribution to the surface plasmon intensity [($J_{\mathrm{tot}}(z=0)$ in Fig. 4(a)], the above ratio is drastically changed (≈1:0.12:−0.24) and the intrinsic contribution is most dominant. This is because the core-hole potential in the photoemission final state is felt by the surface electrons more strongly when the core hole is located at the surface. This causes the enhancement of the intrinsic surface plasmon. The relative intensity of the intrinsic plasmon decreases for photoemission from inside the solid ($z>0$) since the core-hole potential interacts weakly with the surface electrons, and the extrinsic plasmon intensity, which increases with the path length, dominates. The large difference in the ratio of the different plasmon contributions between J_{tot} and $J_{\mathrm{tot}}(z=0)$ makes it imperative to determine the ratios using a different approach.

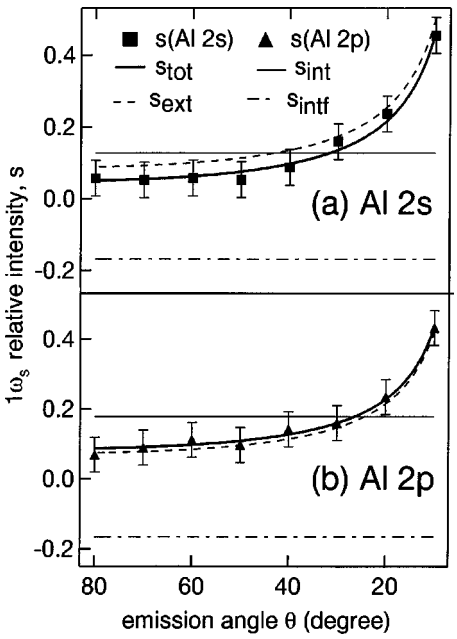

FIG. 5. Variation of the surface plasmon relative intensity s (which is normalized to the no-loss peak), as function of emission angle for (a) Al $2s$ and (b) Al $2p$. A fit to the experimental data (thick solid line) gives the intrinsic (thin solid line), extrinsic (dashed line), and interference (dot-dashed line) contributions to the surface plasmon intensity.

C. Surface plasmon intensity variation

The relative intensity (s) variation of $1\omega_s$ as a function of the emission angle (Fig. 5) can give quantitative estimates of the intrinsic and extrinsic processes and resolve the uncertainty in the ratio of different plasmon contributions discussed above. s shows an increasing trend with decreasing θ for both Al $2s$ and $2p$ (Figs. 5 and 2). Bradshaw *et al.* calculated the angular dependence of the Al related surface plasmon intensity in the XPS spectra of oxygen adsorbed on Al using a semiclassical approach.[7] In the limit of large photoelectron velocity they found that the extrinsic term (s_{ext}) is

inversely proportional to the perpendicular component of the velocity of the photoelectron. Thus in grazing emission, where the perpendicular component of the photoelectron velocity decreases, the extrinsic plasmon intensity is enhanced and the θ dependence of s_{ext} turns out to be $1/\sin\theta$. The intrinsic (s_{int}) and interference (s_{intf}) processes are independent of θ because they do not depend on the trajectory of the outgoing photoelectron. For high velocities of the outgoing photoelectron, the following expression has been obtained for s by Bradshaw *et al.*:[7]

$$s = s_{int} + s_{ext} + s_{intf}, \tag{9}$$

where

$$s_{int} = c_1 c_2, \quad s_{ext} = c_1 \frac{\pi e^2}{4v \sin\theta}, \quad \text{and} \quad s_{intf} = c_1 c_3 \frac{\pi e^2}{2v}.$$

In the above equations, v is the velocity of the outgoing photoelectron with charge e, and c_i ($i=1,2,3$) are the parameters for the model. The deviation of c_1 from unity quantifies the difference of the suggested model from reality; c_2 gives the relative magnitude of the intrinsic effect and $c_3 \approx 1$ for sufficiently high v.[7] The $\pi e^2/2v$ factor is calculated to be 0.172 and 0.169 corresponding to Al $2s$ and $2p$. The c_i parameters are obtained from the least square fitting of the experimental data in Fig. 5 with Eq. (9). Although this model is for plasmons generated by atoms adsorbed on the surface, we apply Eq. (9) for Al $2p$ and $2s$ related surface plasmons to examine whether the contribution from surface photoemission dominates the surface plasmon intensity (as indicated by $[J_{tot}(z=0)]$ in Fig. 4). In fact, a good fit to the experimental data has been obtained using the above expression (s_{tot} in Fig. 5). We obtain $c_1 = 1.01\,(0.87)$, $c_2 = 0.13\,(0.21)$, and $c_3 = 0.97\,(1.13)$ for the Al $2s$ ($2p$) surface plasmon. The closeness of c_1 to unity indicates that the model given by Bradshaw *et al.* can indeed describe the angular variation of the Al surface plasmon in the high velocity limit ($c_3 \approx 1$). It should be noted that the value of c_1 obtained by Bradshaw *et al.* for the Al surface plasmon excited by adsorbed oxygen was 0.27, resulting in $s_{int} = 0.04$. This small value of s_{int} was attributed by the authors to the weakness of coupling between the adsorbate and substrate due to the cloud of oxygen valence electrons, which isolates the core hole from the conduction electrons, making the screening less effective.

The s_{int} values found by us for Al(111) from the fitting are 0.13 and 0.18 for Al $2s$ and $2p$, respectively (Fig. 5). s_{int} is higher for Al $2p$, probably because the intra-atomic screening is more efficient for the deeper Al $2s$ core level, so that the free conduction electrons feel the core-hole potential less (hence the intrinsic plasmon intensity is less) than in the case of the shallower Al $2p$ core level. The contribution of the interference process (s_{intf}) is found to be negative (-0.17) for both Al $2s$ and $2p$ (Fig. 5). The magnitude of s_{intf} is comparable to the intrinsic term, and significantly reduces the intensity of the surface plasmons. As discussed earlier, the variation of the $1\omega_s$ intensity with θ is because of the extrinsic plasmon contribution (dashed lines in Fig. 5) which varies as $1/\sin\theta$. Hence in grazing emission, s_{ext} dominates

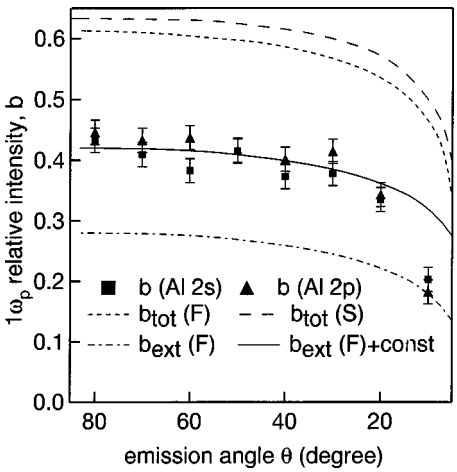

FIG. 6. Variation of Al $2s$ and Al $2p$ related bulk plasmon relative intensity b (which is normalized to the no-loss peak), as function of emission angle is compared with the calculations from Baird *et al.* (Ref. 6) (see the text).

(0.45 for Al $2s$ and 0.43 for Al $2p$), and above $\approx 40°$ (25°) s_{ext} becomes smaller than s_{int}.

From the present analysis, in normal emission the ratio of intrinsic, extrinsic, and interference contributions to the surface plasmon intensity turns out to be 1:0.7:-1.3 for Al $2s$ (1:0.4:-0.9 for Al $2p$). The intrinsic to extrinsic plasmon ratio obtained here is in relatively better agreement with the ratio 1:0.12 obtained from the $z=0$ surface plasmon line shape calculation $[J_{tot}(z=0)]$ rather than the 1:3.6 ratio from the integrated $1\omega_s$ line shape (J_{tot}). This indicates that contribution of surface photoemission to the $1\omega_s$ intensity is underestimated by J_{tot}. In grazing emission, this ratio is 1:3.6:-1.3 for Al $2s$ (1:2.4:-0.9 for Al $2p$), indicating a 5–6 times enhancement of the extrinsic plasmon contribution. The magnitude of the interference term compared to the sum of extrinsic and intrinsic contributions is as high as 76% (for Al $2s$) in normal emission and decreases to 28% in grazing emission.

We propose that the experimentally observed changes in the $1\omega_s$ line shape (as shown in Figs. 1–3), from highly asymmetric in normal emission to relatively more symmetric in grazing emission, could be related to the large enhancement of the extrinsic surface plasmon in grazing emission. The sharply peaked asymmetric line shape of the intrinsic plasmon compared to the broad line shape of the extrinsic plasmon [Fig. 4(b)] supports this proposition. This explanation is also supported by the observation of symmetric plasmon line shape in EELS, where only extrinsic plasmons are excited.[27] However, a calculation of the surface plasmon line shape as a function of θ, which does not exist in the literature, is required for providing a definitive answer.

D. Bulk plasmon intensity variation

The relative intensities of the $1\omega_p$ bulk plasmon (b) for Al $2s$ and $2p$ decrease marginally (from 0.45 to 0.4) between normal and 30° (Fig. 6). Below $\theta = 30°$, b decreases rapidly and is about 0.2 at $\theta = 10°$. Baird *et al.*[8] calculated the varia-

tion of b with θ, and we compare the present experimental data with those results (see Fig. 6). $b_{\mathrm{tot}}(F)$ was calculated by Baird *et al.* using the method suggested by Feibelman,[16] which assumes infinite core-hole lifetime and a smooth cutoff at the critical wave vector (q_c). $b_{\mathrm{tot}}(S)$ was calculated by the method suggested by Šunjić and co-workers[18,19] which assumes a finite core-hole lifetime and a sharp cutoff at q_c. Both the methods are based on jellium model and use the semiclassical model of electron-electron interaction. $b_{\mathrm{ext}}(F)$ was calculated by Feibelman's method considering only the extrinsic plasmon contribution.[8] From the comparison of theory[8] and present data, although the θ variation is similar, it is clear that both the methods (F and S) overestimate the intrinsic plasmon contribution. On the other hand, $b_{\mathrm{ext}}(F)$ lies below the experimental data because the intrinsic and interference contributions are not included in this calculation. As in the case of surface plasmons, if we consider that the intrinsic and interference terms are θ independent, the addition of a constant term to $b_{\mathrm{ext}}(F)$ should be able to simulate the experimental data. This constant value, which gives a quantitative estimate of the sum of intrinsic and interference contributions, turns out to be 0.14, and gives a reasonable fit to the experimental data (solid line in Fig. 6). This value has been used by us to estimate the intrinsic bulk plasmon probability (discussed later).

In order to obtain quantitative estimates of the intrinsic, extrinsic, and interference processes in bulk plasmons, we have studied the Al $2s$ core-level spectrum over a wide kinetic energy range. The spectrum clearly shows the bulk plasmon peaks at 15.4, 30.8, 46.2, 62, 76.6, and 92.6 eV loss energies corresponding to multiple ($n=1-6$) bulk plasmon ($n\omega_p$) excitations (Fig. 7). The main peak is truncated to show the plasmon region in an expanded scale. Besides the bulk plasmon peaks, $1\omega_s$ (at 10.4 eV loss energy) and multiple bulk and surface plasmons excitations towards higher loss energies like $2\omega_s$, $1\omega_p+1\omega_s$, $2\omega_p+1\omega_s$, and $3\omega_p+1\omega_s$ are indicated sequentially (from lower to higher loss energy) by arrows in Fig. 7. The energies of the $3\omega_p$ and $4\omega_p$ excitations corresponding to Al $2p$ are shown with slanted arrows. We find that the intensity contribution from Al $2p$ related $3\omega_p$, which almost coincides with the Al $2s$ main peak, to be about 6% compared to the main peak. The fit to the experimental data, where each of the above mentioned plasmon features are fitted with asymmetric Lorentzians, is shown by a solid line through the data points. From the fitting we find that Γ_L is larger than Γ_R and both these widths increase steeply with n and shows a saturating trend for $n\geqslant 5$ (inset, Fig. 7). The increase in width, for example, for $2\omega_p$, is due to the excitation of $2\omega_p$ photoelectrons through a second plasmon excitation by $1\omega_p$ photoelectrons. Thus the $2\omega_p$ line shape can be approximated to be the self-convolution of the $1\omega_p$ line shape.[3] The asymmetry of the bulk plasmon line shape, quantified by $\kappa\,(=\Gamma_L/\Gamma_R=2.5)$, is independent of n. Thus, although the width increases with n, the bulk plasmon asymmetry remains unchanged. Interestingly, this is in contrast to the systematic change in asymmetry (κ) as a function of θ observed for both surface and bulk plasmon (as discussed in Sec. III A).

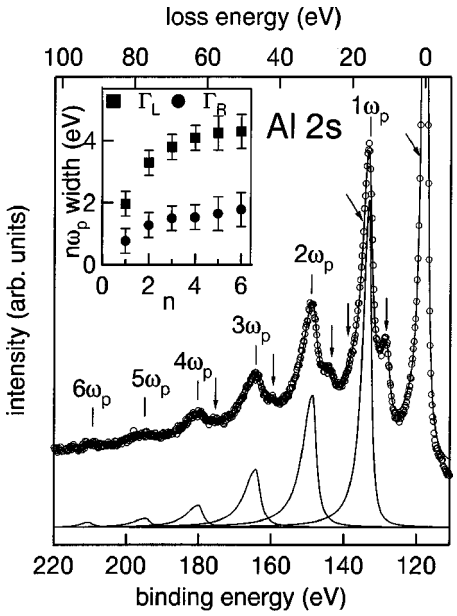

FIG. 7. Wide range Al $2s$ core-level spectrum recorded at $\theta=45°$ (experiment: open circles; fit: solid line through experimental data) showing multiple ($n=1-6$) bulk plasmon excitations ($n\omega_p$). Vertical arrows indicate the energy positions of the multiple bulk and surface plasmon excitations related to Al $2s$, while the slanted arrows show the energy positions of $3\omega_p$ and $4\omega_p$ excitations related to Al $2p$ (see the text). The deconvoluted $n\omega_p$ line shapes (solid lines) are shown at the bottom. The inset shows the variations of $n\omega_p$ left (Γ_L, filled square) and right (Γ_R, filled circle) Lorentzian widths as functions of n.

The variation of the $n\omega_p$ relative intensity as a function of n $[b(n)]$ has been studied by different groups to determine the relative extrinsic and intrinsic contributions to the bulk plasmon. However, the results from the different studies[1,3,6,5,20] are not in agreement. The combined effect of intrinsic and extrinsic plasmon in the $n\omega_p$ intensity variation was suggested by Langreth[17] to be

$$b(n)=\alpha^n\sum_{m=0}^{n}\frac{(\beta/\alpha)^m}{m!}, \tag{10}$$

where α is the extrinsic plasmon creation probability. β is the measure of probability $[P_{\mathrm{int}}(n)]$ of the intrinsic excitation of n plasmons given by

$$P_{\mathrm{int}}(n)=e^{-\beta}\frac{\beta^n}{n!}. \tag{11}$$

Based on perturbation theory arguments in momentum space, Chang and Langreth[14] suggested that the strength of extrinsic plasmons for $n\omega_p$ should vary as α^n, where α is about 0.5. Based on Eq. (10), van Attekum *et al.*[5] found the Al $2s$ related intrinsic bulk plasmon component to be 25% ($\beta=0.21,\alpha=0.62$) of the total plasmon intensity. Using a similar procedure, Steiner *et al.*[6] determined β and α in Al to be 0.11 and 0.66, respectively, and thus the intrinsic plasmon was a factor of 2 lower than that estimated by van Attekum *et al.*[5] Neither of these studies[5,6] considered the interference

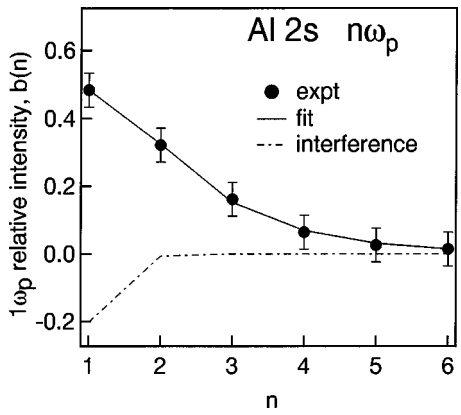

FIG. 8. Variation of $n\omega_p$ intensity (filled circles) as a function of n ($n=1-6$). The solid line is a fit to the data, and the dot-dashed line is the interference contribution.

effect. Pardee *et al.*[3] could simulate the $n\omega_p$ intensity variation using a random spatial emission model for the extrinsic plasmon probability,[15] and concluded that the intrinsic plasmon is almost nonexistent. Based on a theory including plasmon dispersion, Steiner *et al.* obtained the β and α values to be 0.11 and 0.63 for Al.[6] On the contrary, Lundqvist suggested a 50% contribution of the intrinsic plasmon while Penn obtained a value of 26% based on theoretical calculations without considering the interference effect.[1,20]

Because of the disagreement in the literature about the intrinsic plasmon probability, the variation of $b(n)$ [the area under the deconvoluted bulk plasmon line-shapes (bottom of Fig. 7) relative to the main peak] has been studied by us (Fig. 8). Since the plasmon areas may depend on the method of background subtraction, we have used different background substraction methods (Tougaard, linear, and constant). Tougaard background subtraction, which describes the inelastic background in many metals to a reasonable approximation,[29] has been performed on the data presented in Fig. 8. Surprisingly, a fit to the data with Eq. (10) gives an unphysical negative value for the intrinsic plasmon strength (β), irrespective of the method of background subtraction. Moreover, attempt to fit the data assuming only extrinsic plasmon contribution following the method of Pardee *et al.*[3] did not succeed.

In order to resolve the issue of negative β we noted that, besides the intrinsic and extrinsic plasmons, a sizable negative contribution to the bulk plasmon intensity arises from the interference term.[23] It was suggested by Chang and Langreth that the interference term can be included in Eq. (10) by replacing β with $\beta+(e^2/\hbar v)\chi$, where $e^2/\hbar v$ is a coupling constant dependent on the velocity v of the photoelectron and χ is related to the probability of the interference effect.[14] Since the interference effect is between intrinsic and extrinsic plasmons, it is reasonable to assume that its probability would be proportional to the product of intrinsic and extrinsic plasmon probabilities. Hence χ is taken to be

$$\chi = c\,\alpha^n e^{-\beta}\beta^n/n!, \tag{12}$$

where c is the proportionality constant. Thus we have used a modified Langreth equation for $b(n)$ given by

$$b(n) = \alpha^n \sum_{m=0}^{n} \frac{[(\beta-0.11\chi)/\alpha]^m}{m!} \tag{13}$$

to fit the data in Fig. 8, where 0.11 is the value of the coupling constant for Al 2s photoelectrons. By varying α, β, and c, we obtain a good fit to the experimental data (solid line in Fig. 8) with a positive value for β (=0.22) and $\alpha=0.46$. The value of α obtained by us is close to the theoretically suggested value of 0.5, and thus supports the perturbation theory based model of Chang and Langreth.[14] The interference term is negative with a decreasing contribution for higher n (dot-dashed line in Fig. 8). The variation of α and β for the different methods of background subtraction is about 15%, and the contribution from the interference term is always negative.

We obtain the ratio of the intrinsic to extrinsic plasmon probabilities for $1\omega_p$ to be 0.18:0.46 [$=e^{-\beta}\beta:\alpha$ from Eq. (11)] and for $2\omega_p$ to be 0.02:0.21 [$=e^{-\beta}\beta^2/2!:\alpha^2$]. Thus, for $1\omega_p$, the ratio of intrinsic to extrinsic plasmon contribution is about 1:2.6, and that for $2\omega_p$ turns out to be 1:11. This indicates that the probability of exciting two or more intrinsic bulk plasmons is indeed small. This is also the reason why the interference contribution, whose probability is proportional to the product of intrinsic and extrinsic plasmon probabilities, is small for multiple plasmon excitations with $n\geqslant 2$ (Fig. 8). We would like to comment that the disagreement in the previously reported[3,5,6] experiment based estimates of β and α probably arises from the methods of data analysis. The deconvolution of the experimental data from instrumental broadening, the use of a DS line shape for the main peak and asymmetric Lorentzians for the plasmons, Tougaard background subtraction, and finally the introduction of the interference term in the Langreth equation have been used to obtain the present values of β and α for Al.

In order to further check the validity of the above result, we have calculated the $1\omega_p$ line shape and the intrinsic, extrinsic, and interference contributions using the following expression derived by Inglesfield[22] based on perturbation theory (as discussed in Sec. III B for a surface plasmon):

$$J_{\rm tot}(\omega,z) = \frac{2\omega_p^2}{\beta^2\pi}\int_0^{K_{\rm max}} \frac{k_\parallel dk_\parallel}{q(k_\parallel^2+q^2)}|X|^2, \tag{14}$$

where $k_\parallel^2+q^2=K_{\rm max}^2$. In the above expression, q is the bulk plasmon momentum and $K_{\rm max}$ is the cutoff wave vector (0.5 a.u.). X is the combination of seven terms where the first six terms correspond to extrinsic contribution and the last term corresponds to the intrinsic contribution (see Eq. 24 of Ref. 22) The calculated line shape is asymmetric and is in good agreement with experiment.[43] The ratio of the integrated areas under the calculated intrinsic, extrinsic, and interference plasmon line shapes turns out to be 1:2.4:$-$0.35. Thus the intrinsic to extrinsic bulk plasmon ratio is 1:2.4, which is in very good agreement with the ratio 1:2.6 obtained from the fitting of the experimental $n\omega_p$ intensities with modified Langreth equation [Eq. (13)]. Moreover, using the above ratio of the intrinsic to interference effect (1:$-$.35) and their sum to be 0.14 (from Fig. 6), the probability of the intrinsic term turns out to be 0.21 which is in good agreement with

0.18 obtained from the $n\omega_p$ intensity variation. The satisfying agreement of the different approaches shows the reliability of the extrinsic and intrinsic plasmon probabilities obtained by us and the success of nearly free electron model based theories in explaining the collective excitations in Al.

IV. CONCLUSION

The surface plasmon ($1\omega_s$) excitation in the core-level spectra of Al(111) is found to change from a highly asymmetric to a more symmetric line shape from normal to grazing emission, which is probably due to the large enhancement of the extrinsic plasmon intensity in grazing emission. The $1\omega_s$ line shape has been calculated following the perturbation based theory of Inglesfield.[22] The experimentally observed steplike surface plasmon line shape in normal emission is well reproduced by theory. However, the disagreement on the higher loss energy side is probably due to the underestimation of the surface photoemission contribution to the $1\omega_s$ intensity or the existence of a broad featureless multipole plasmon excitation. The interference effect always gives a negative contribution to the plasmon intensity and plays an important role in determining the surface plasmon intensity and line shape. For example, it reduces the intensity and makes the line shape relatively more symmetric. The variation of $1\omega_s$ intensity with θ could be explained on the basis of the semiclassical model proposed by Bradshaw *et al.*[7] The ratio of intrinsic, extrinsic, and interference contributions is found to be 1:0.7:−1.3 in normal emission and 1:3.6:−1.3 in grazing emission for the Al 2*s* related surface plasmon.

Although not as pronounced as the surface plasmon, the bulk plasmon ($1\omega_p$) line shape is asymmetric in normal emission and becomes nearly symmetric in grazing emission. The Al 2*s* multiple bulk plasmons ($n\omega_p$) increase in width with *n*, although the asymmetry of the line shape does not change. The importance of the interference effect in the bulk plasmon is evident from the intensity variation of $n\omega_p$ as a function of *n*, where, unless the interference term is taken into account, the intrinsic plasmon probability is negative. An intrinsic to extrinsic plasmon ratio of 1:2.6 is obtained for $1\omega_p$, which is in very good agreement with that obtained from the perturbation based theoretical line-shape calculations (1:2.4). Thus reliable estimates of the intrinsic and extrinsic bulk plasmons in Al have been obtained.

ACKNOWLEDGMENTS

Professor K. Horn, Dr. B. A. Dasannacharya, and Professor A. Gupta are thanked for support. A part of the work was supported by DST Project No. SP/S2/M-06/99. A.K.S. and S.B. are thankful to DST for financial support.

*Email address:
barman@iucindore.ernet.in; srbarman@mailcity.com

[1] B. I. Lundqvist, Phys. Kondens. Mater. **9**, 236 (1969).
[2] D. C. Langreth, Phys. Rev. Lett. **26**, 1229 (1971).
[3] W. J. Pardee, G. D. Mahan, D. E. Eastman, R. A. Pollak, L. Ley, F. R. McFeely, S. P. Kowalczky, and D. A. Shirley, Phys. Rev. B **11**, 3614 (1975).
[4] J. C. Fuggle, D. J. Fabian, and L. M. Watson, J. Electron Spectrosc. Relat. Phenom. **9**, 99 (1976).
[5] P. M. Th. van Attekum and J. M. Trooster, Phys. Rev. B **18**, 3872 (1978); Phys. Rev. B **20**, 2335 (1979).
[6] P. Steiner, H. Höechst, and S. Hüfner, Z. Phys. B: Condens. Matter **30**, 129 (1978); H. Höechst, P. Steiner, and S. Hüfner, *ibid.* **30**, 145 (1978).
[7] A. M. Bradshaw, W. Domcke, and L. S. Cederbaum, Phys. Rev. B **16**, 1480 (1977).
[8] R. J. Baird, C. S. Fadley, S. M. Goldberg, P. J. Feibelman, and M. Šunjić, Surf. Sci. **72**, 495 (1978).
[9] N. V. Smith and W. E. Spicer, Phys. Rev. Lett. **23**, 769 (1969).
[10] Y. Baer and G. Busch, Phys. Rev. Lett. **30**, 280 (1973); P. H. Citrin, G. K. Wertheim, and Y. Baer, Phys. Rev. B **16**, 4256 (1977).
[11] S. P. Kowalczky, L. Ley, F. R. McFeely, R. A. Pollak, and D. A. Shirley, Phys. Rev. B **8**, 3583 (1973); R. A. Pollak, L. Ley, F. R. McFeely, S. P. Kowalczky, and D. A. Shirley, J. Electron Spectrosc. Relat. Phenom. **3**, 381 (1974).
[12] S. A. Flodström, R. Z. Bachrach, R. S. Bauer, J. C. McMenamin, and S. B. M. Hagström, J. Vac. Sci. Technol. **14**, 303 (1977).
[13] D. Norman and D. P. Woodruff, Surf. Sci. **79**, 76 (1979).
[14] J. J. Chang and D. C. Langreth, Phys. Rev. B **5**, 3512 (1972); **8**, 4638 (1973).
[15] G. D. Mahan, Phys. Status Solidi B **55**, 703 (1973).
[16] P. J. Feibelman, Phys. Rev. B **7**, 2305 (1973).
[17] D. C. Langreth, in *Collective Properties of Physical Systems*, edited by B. Lundquist and S. Lundquist (Academic, New York, 1974).
[18] M. Šunjić, D. Šokčević, and A. Lucas, J. Electron Spectrosc. Relat. Phenom. **5**, 963 (1974).
[19] M. Šunjić and D. Šokčević, Solid State Commun. **15**, 165 (1974); D. Šokčević and M. Šunjić, *ibid.* **15**, 1703 (1974).
[20] D. R. Penn, Phys. Rev. Lett. **38**, 1429 (1977); **40**, 568 (1978).
[21] J. E. Inglesfield, Solid State Commun. **40**, 467 (1981).
[22] J. E. Inglesfield, J. Phys. C **16**, 403 (1983).
[23] S. M. Bose, S. Prutzer, and P. Longe, Phys. Rev. B **27**, 5992 (1983).
[24] L. H. Hedin, in *X-Ray Spectroscopy*, edited by L. V. Azaroff (McGraw-Hill, New York, 1974), p. 226.
[25] A. Liebsch, *Elementary Excitation on Metal Surfaces* (Plenum, New York, 1997).
[26] E. W. Plummer, Solid State Commun. **84**, 143 (1992).
[27] G. Chiarello, V. Formoso, A. Santaniello, E. Colavita, and L. Papagno, Phys. Rev. B **62**, 12676 (2000).
[28] M. Cardona and L. Ley, *Photoemission in Solids* (Springer-Verlag, Berlin, 1978).
[29] S. Tougaard, Surf. Sci. **216**, 343 (1989); C. Jansson, H. S. Hansen, F. Yubero, and S. Tougaard, J. Electron Spectrosc. Relat. Phenom. **60**, 301 (1992).
[30] S. Doniach and M. Šunjić, J. Phys. C **3**, 287 (1970).
[31] W. Theis and K. Horn, Phys. Rev. B **47**, 16 060 (1993).
[32] M. T. Sieger, T. Miller, and T.-C. Chiang, Phys. Rev. Lett. **75**, 2043 (1995); T. E. H. Walker and J. T. Waber, J. Phys. B **7**, 674 (1974); G. M. Bancroft, W. Gudat, and D. E. Eastman, Phys. Rev. B **17**, 4499 (1978).

[33] C. O. Alambladh and U. von Barth, Phys. Rev. B **13**, 3307 (1976); P. Minnhagen, J. Phys. F: Met. Phys. **7**, 2441 (1977); G. W. Bryant and G. D. Mahan, Phys. Rev. B **17**, 1744 (1978).
[34] M. S. Banna and D. A. Shirley, J. Electron Spectrosc. Relat. Phenom. **8**, 255 (1976).
[35] R. H. Ritchie, Prog. Theor. Phys. **29**, 607 (1963).
[36] A. J. Bennett, Phys. Rev. B **1**, 203 (1970); L. Kleinman, *ibid.* **7**, 2288 (1973); D. Pines, Phys. Rev. **92**, 626 (1953).
[37] M. P. Seah and W. A. Dench, Surf. Interface Anal. **1**, 2 (1979).
[38] H. Ishida and A. Liebsch, Phys. Rev. B **54**, 14127 (1996).
[39] P. J. Feibelman, Prog. Surf. Sci. **12**, 287 (1982); F. Flores and F. García-Moliner, Solid State Commun. **11**, 1295 (1972); J. Harris and A. Griffin, Phys. Lett. **34A**, 51 (1971).
[40] H. J. Levinson, E. W. Plummer, and P. J. Feibelman, Phys. Rev. Lett. **43**, 952 (1979).
[41] S. R. Barman, P. Häberle, and K. Horn, Phys. Rev. B **58**, R4285 (1998); S. R. Barman, C. Stampfl, P. Haeberle, W. Ibanez, Y. Q. Cai, and K. Horn, *ibid.* **64**, 195410 (2001).
[42] J. W. Gadzuk, J. Electron Spectrosc. Relat. Phenom. **11**, 355 (1977).
[43] C. Biswas, A. K. Shukla, S. Banik, V. K. Ahire, and S. R. Barman (unpublished).